

Molecular Physics

An International Journal at the Interface Between Chemistry and Physics

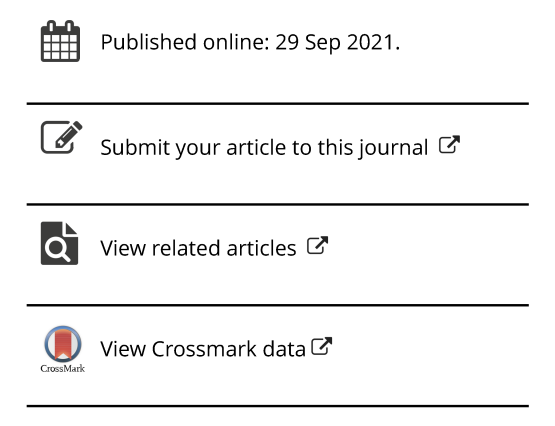
ISSN: (Print) (Online) Journal homepage: https://www.tandfonline.com/loi/tmph20

Dissociative electron attachment in C₂H via electronic resonances

Sahil Gulania & Anna I. Krylov

To cite this article: Sahil Gulania & Anna I. Krylov (2021): Dissociative electron attachment in C_2H via electronic resonances, Molecular Physics, DOI: $\underline{10.1080/00268976.2021.1979262}$

To link to this article: https://doi.org/10.1080/00268976.2021.1979262





JOHN STANTON SPECIAL ISSUE: THEORY MEETS EXPERIMENT



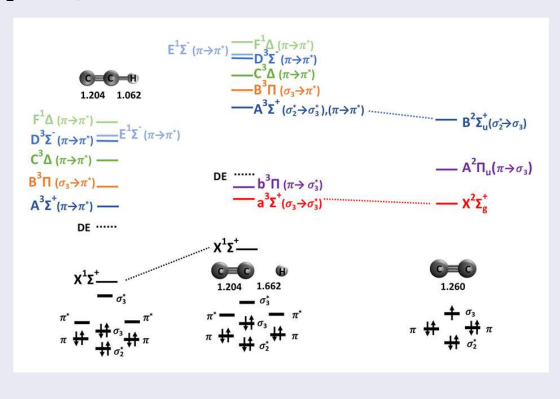
Dissociative electron attachment in C₂H via electronic resonances

Sahil Gulania D and Anna I. Krylov D

Department of Chemistry, University of Southern California, Los Angeles, CA, USA

ARSTRACT

Investigation of microwave-activated CH₄/H₂ plasma used in chemical vapour deposition of diamond revealed the presence of electronically excited C_2^{-*} ($B^2 \Sigma_u^+$). Using high-level electronic structure methods, we investigate electronic structure of C_2H^- and suggest possible routes for the formation of C_2^- in the ground ($X^2 \Sigma_g^+$) and excited ($B^2 \Sigma_u^+$) states via electronic resonances. To describe electronically metastable states, we employ the equation-of-motion coupled-cluster method augmented by the complex absorbing potential. The resonance wavefunctions are analysed using natural transition orbitals. We identified several resonances in C_2H^- , including the state that may lead to C_2^{-*} ($B^2 \Sigma_u^+$).



KEYWORDS

Electronic resonance; EOM-CCSD; Plasma physics; Non-Hermitian quantum mechanics; Dissociative electron attachment

1. Introduction

In high-energy environments, electrons have sufficient energy to overcome their attraction to the nuclei, giving rise to a fourth state of matter: plasma. Plasma consists of charged particles (electrons, ions) and metastable atomic and molecular species. Plasma constitutes 99.999% of the visible universe, as it is the main component of stars. In our everyday lives, plasma is generated by electric discharge such as in lightning or in plasma TVs. Cosmic radiation produces plasmas in the atmosphere, giving rise to the northern lights. Plasma can also be generated in the course of decomposition of energetic materials.

Plasma can play an important role in chemistry. Free electrons can attach themselves to molecules forming stable or transient anions. Depending on the type of orbital to which the electron attaches different types of structural transformations ensue. This electron-induced chemistry [1,2] is akin to photochemistry [3], wherein the bonding pattern of a molecule is altered by promoting electrons from occupied to virtual orbitals. An example of an electron-induced reaction is dissociative electron attachment (DEA), in which molecules fall apart upon the attachment of an electron [4–7]. DEA occurs in interstellar media, planetary atmospheres, radiolysis, and in plasma reactors. One fascinating example [8,9] of DEA is double-strand breaking in DNA by slow electrons: electrons with energies as low as 1–2 eV can break two covalent bonds (of total energy ~ 10 eV) in DNA. In these examples, DEA (or, more generally, plasma-induced processes) are of a destructive

nature: plasma breaks molecules apart. Significant efforts have been directed towards controlling and mitigating such electron-induced processes in fusion reactors and in cases of matter exposed to high-energy radiation. In contrast, some technologies exploit the destructive ability of plasma to clean NOx and SOx from the exhaust of power plants and engines as well to remove organic pollutants from contaminated water [10–14], or in nanostructuring through electron beam lithography [15].

Recently, significant efforts have been directed towards exploiting plasma-induced chemistry in a more constructive way, for example, to use electrons for making new molecules that are difficult to make by other means. One historic example of that nature is nitrogen fixation by electric arc – before the Haber–Bosch process was developed to its full potential, the Birkeland–Eyde process was used on an industrial scale. If we can use plasma for converting nitrogen into chemically bound forms [14], then, perhaps, we can use electrons to facilitate such stubborn processes as methane activation [16–18] of carbon dioxide reduction [19].

The idea of electron catalysis has been around for quite some time [2,12,20,21], yet there are no examples of new, controlled chemistry deliberately achieved via electron attachment. The challenge in developing new chemistry is that we do not understand processes initiated by electron attachment to even rather small molecules. Superficially, electron-induced processes are similar to photochemistry, which is a mature field: there are many established photochemical synthetic reactions, e.g. electrocyclic and Norrish reactions, routinely used in the lab and even on an industrial scale. Quantum chemistry, both conceptual (molecular orbital theory) and quantitative, has been instrumental for developing a mechanistic understanding of photochemistry [3]. However, this arsenal of tools cannot be routinely applied to study DEA because of the nature of the initial state, which is metastable with respect to electron ejection. This metastable nature is the main stumbling block for the theoretical modelling of electron-induced processes.

States that are metastable with respect to electron detachment are called resonances [7,22–25]; they have finite lifetime and decay by ejecting an electron. Hence, resonances are located above the electron detachment (or ionisation) threshold and belong to the continuum part of the spectra. Resonances play an important role in plasma physics, atmospheric chemistry, fusion reactors, interstellar medium, and in many other environments. These states can be produced by electronic excitation, ionisation, or electron attachment. Recent theoretical developments have extended standard quantum chemistry approaches, such as equation-of-motion coupled-cluster (EOM-CC) [26–28] and algebraic diagrammatic

construction [29] theories, to treating resonances [25], by using non-Hermitian quantum mechanics framework [22,24,25,30]. These tools (as well as related CAP-SAC-CI methods [31]) have been used to study a variety of processes, ranging from spectroscopy of stable and transient anions [32–34], possible routes of astrochemical formation of cyano-polyyne anions [35], DEA in chloroethylenes [36], and electron-transfer reactions [37].

In this contribution, we employ EOM-CC methods [26–28] augmented with the complex absorbing potential (CAP) [25,38,39] to interrogate electronic structure and DEA in C_2H^- . This study is motivated by the observation of electronically excited C_2^- (detected via fluorescence) in carbon-rich plasmas [40], such as microwaveactivated plasma in chemical vapour deposition (CVD) of diamond. C_2H^- is also relevant for astrochemistry, along with other molecular anions detected in interstellar medium and planetary atmospheres, such as CN^- , $C_{2n}H^-$, $C_{2n+1}N^-$, benzonitrile, etc [41–47].

Although C_2^- is commonly occurring in many highenergy environments [40,48–50], the mechanism of its formation is not fully understood. From the observed spatial distribution and its variation with changes in process conditions, the experimentalists deduced [40] that both ground- and excited-state C_2^- ($X^2\Sigma_g^+$ and $B^2\Sigma_u^+$, respectively) are formed directly via DEA to C_2H :

$$C_2H + e \rightarrow C_2^{-*}/C_2^{-} + H.$$
 (1)

 C_2^- is also formed by the DEA to acetylene [51], but it was concluded [40] that this channel is predominantly responsible for the production of the ground-state species. The authors [40] have also ruled out the formation of C_2^{-*} by other processes, such as electron attachment to C_2 or electron-impact excitation of C_2^- . The conclusion of this detailed analysis is well supported by the data [40], however, no explanation was given of how exactly electronically excited C_2^{-*} is formed. The goal of our study is to clarify this issue. We report the calculations of bound and metastable states of C₂H⁻. By using wave-function analysis tools, we identified orbital character of the computed resonances. The main finding is that at the neutral ground-state geometry of C2H, the anion has several resonances of $\pi \to \pi^*$ type, but none of them has antibonding character along the C-H bond and none correlates with the excited C_2^{-*} ($B^2\Sigma_u^+$). The states that can lead to the CH bond dissociation appear only when the C-H bond is elongated, including the resonance that correlates with the $B^2\Sigma_u^+$ state of C_2^- . The implications of this observation and similarities with other DEA processes [9] are discussed below.

In what follows we first describe methods and computational protocols, followed by the discussion of electronic structure of C_2^- and C_2H^- . We then discuss potential energy scans and correlation diagram along the C-H bond and discuss possible mechanism of C_2^{-*} formation.

2. Theoretical methods and computational details

EOM-CC framework enables treating diverse types of electronic structure [26-28,52-58], including electronically excited and open-shell species [59]. EOM-CC produces size-intensive transition energies for electronic excitations, ionisation, or attachment [60]. It treats nondynamic and dynamic correlation in a single computational step and its accuracy can be systematically improved up to the exact solution [60]. The major advantage of EOM-CC is its ability to treat different types of states in a balanced fashion by employing the same model Hamiltonian (similarity transformed *H*). In particular, EOM-CC describes closed- and open-shell species on an equal footing, which enables meaningful comparisons of the energies of the anionic and the neutral states, as well as metastable and near-threshold bound states.

Here we apply EOM-CCSD to investigate the electronic spectrum of C₂H⁻ below and above the electrondetachment continuum onset. Figure 1 illustrates the target-state manifolds accessed by EOM-EE and EOM-IP. In both calculations the same closed-shell reference state is used; consequently all relevant states are represented with the same set of orbitals and computed using the same effective Hamiltonian,

$$\bar{H} \equiv e^{-\hat{T}} \hat{H} e^{\hat{T}},\tag{2}$$

where operator \hat{T} comprises coupled-cluster amplitudes of the reference state. Here, the reference wave function corresponds to the closed-shell ground-state CCSD solution for the C₂H⁻ (N-electron system). The diagonalisation of \bar{H} in the respective sectors of Fock space yields amplitudes of the EOM operators. We determined the electron-detachment thresholds and properties of the parent neutral radical by the EOM-IP variant of the method in which the target N-1-electron states are described by the EOM operators that remove one electron (i.e. of the 1h and 2h1p types). To study bound excited states, we employed the EOM-EE variant in which the target N-electron states are described by the EOM operators that excite one or two electrons (i.e. 1h1p and 2h2p). In calculations of C_2^{2-} , we used EOM-IP-CCSD with the dianionic reference state (C_2^{2-}) . To describe N-electron metastable states embedded in the electron-detachment continuum, we augment the standard EOM Hamiltonian by CAP [38,39], which gives rise

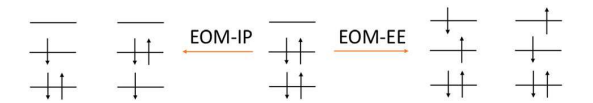


Figure 1. Manifolds of target states accessed by EOM-IP and EOM-EE. In both variants, the same closed-shell reference is used. EOM-IP-CCSD describes open-shell doublet states by employing ionising operators of the 1h and 2h1p types. EOM-EE-CCSD describes electronically excited states by employing electronconserving excitation operators of the 1h1p and 2h2p types.

to the CAP-EOM-EE-CCSD ansatz [25,61-65]. Note that the onset of the continuum in EOM-EE exactly corresponds to the electron detachment energy obtained from EOM-IP, which allows one to unambiguously distinguish between the bound and continuum states.

The CAP [25,38,39,61,62] approach entails augmenting the standard Hamiltonian \hat{H}_0 with an imaginary potential

$$\hat{H}(\eta) = \hat{H}_0 - i\eta \hat{W}(r),\tag{3}$$

where η represents the strength of the CAP. The imaginary potential absorbs the diverging tail of a metastable state making it \mathcal{L}^2 -integrable. The eigen-energies of the CAP-augmented Hamiltonian are complex - the real part is the position of the resonance and the imaginary part is the resonance width (which is inversely proportional to the lifetime of the resonance). In our calculations, the CAP is quadratic with cuboid shape

$$\hat{W}(r) = \hat{W}_x(r_x) + \hat{W}_y(r_y) + \hat{W}_z(r_z), \tag{4}$$

with

$$\hat{W}_{\alpha}(r_{\alpha}) = \begin{cases} 0 & \text{if } |r_{\alpha}| \le r_{\alpha}^{0} \\ (|r_{\alpha}| - r_{\alpha}^{0})^{2} & \text{otherwise,} \end{cases}$$
 (5)

where the coordinates (r_x^0, r_y^0, r_z^0) define the onset of the CAP in each dimension. Following the same protocol as in previous studies [61,62], we fixed the CAP onset at the spatial extent of the wave function for the reference state, $r_{\alpha}^{0} = \sqrt{\langle \Psi_{CCSD} | r_{\alpha}^{2} | \Psi_{CCSD} \rangle}$, where Ψ_{CCSD} is the CCSD solution (CAP-free) for the ground state of the anion. In our calculations here, we include CAP already at the Hartree-Fock level, in contrast to the projective CAP approach used in combination with the SAC-CI ansatz by Ehara and Sommerfeld [31] or with the ADC ansatz by Dreuw and co-workers.

The optimal value of CAP's strength parameter η is determined for each metastable state by calculating η trajectories and searching for the minimum of the function [39,66]:

$$|\eta \frac{\mathrm{d}E(\eta)}{\mathrm{d}\eta}| = min. \tag{6}$$

This procedure minimises the error introduced by the finite-strength of CAP used in incomplete one-electron basis sets. More accurate resonance parameters can be obtained if, instead of considering the raw η -trajectories $E(\eta)$, one analyses the η -trajectories of deperturbed energies $U(\eta)$ from which the explicit dependence of CAP is removed in the first order [62]. The deperturbed complex energies $U(\eta)$ are calculated by subtracting from raw energies $E(\eta)$ the correction $i\eta Tr[\gamma W]$, where γ is the one-particle density matrix of the resonance state. Below we denote the uncorrected energies and widths by $E^{(0)}$ and $\Gamma^{(0)}$ and the respective corrected quantities by $E^{(1)}$ and $\Gamma^{(1)}$.

To analyse the transition properties between the EOM-CCSD states, we employ reduced quantities such as one-particle transition density matrices, natural transition and Dyson orbitals. These objects are related to concrete physical observables and provide a way to derive a molecular orbital picture of the many-body wave functions [67,68]. The one-particle transition density matrix [69–74] (1PTDM) connecting two many-body wave functions Ψ_I and Ψ_I is

$$\gamma_{pq}^{IJ} = \langle \Psi_I | p^{\dagger} q | \Psi_J \rangle , \qquad (7)$$

where operators p^{\dagger} and q denote the creation and annihilation operators corresponding to molecular orbitals ϕ_p and ϕ_q . 1PTDM can be used to compute one-electron transition properties such as oscillator strengths, transition dipole moments, non-adiabatic and mean-field spin-orbit couplings. The norm of γ^{IJ} provides a measure of one-electron character of the transition [75]. The 1PTDM provides a compact representation of the difference between the two states in terms of hole-particle excitations. Singular-value decomposition of γ^{IJ} yields a set of left and right eigenvectors

$$\gamma^{IJ} = U\Sigma V^T, \tag{8}$$

which define hole (ψ_K^h) and particle (ψ_K^e) orbitals corresponding to singular value σ_K (elements of the diagonal matrix Σ)

$$\psi_K^h = \sum_q U_{qK} \phi_q, \tag{9}$$

$$\psi_K^e = \sum_q V_{qK} \phi_q, \tag{10}$$

where ϕ_q denote molecular orbitals of the reference state. Such pairs of hole and particle orbitals are called NTOs (natural transition orbitals). The renormalised squares of singular values (σ_K^2) can be interpreted as weights of each NTO pair in the exciton wave function.

In non-Hermitian formalism, the electronic resonances have complex energy and complex densities whose real and imaginary components are [65]

$$^{Re}\gamma_{pq}^{IJ} = \langle \Psi_{I}^{Re} | p^{\dagger} q | \Psi_{J}^{Re} \rangle - \langle \Psi_{I}^{Im} | p^{\dagger} q | \Psi_{J}^{Im} \rangle , \qquad (11)$$

$${}^{Im}\gamma_{pq}^{IJ} = \langle \Psi_I^{Im} | p^{\dagger} q | \Psi_J^{Re} \rangle + \langle \Psi_I^{Re} | p^{\dagger} q | \Psi_J^{Im} \rangle. \tag{12}$$

The analysis of real part 1PTDM provides information about the orbitals involved in the transition, similar to bound-state analysis. The imaginary part analysis provides insight into the coupling of the resonance with the continuum and its decay channels [65].

2.1. Computational details

All calculations were performed using the Q-Chem electronic structure programme [76,77]. The geometry optimisations of C₂H and its anion were performed with EOM-IP-CCSD and CCSD, respectively, using the augcc-pVTZ basis set [78,79]. Electronic states of the neutral C2H at the neutral and anionic geometries were computed using EOM-IP-CCSD, as electron detachment from C₂H⁻. The aug-cc-pVTZ basis set was further augmented by the 3s3p1d diffuse functions on carbons and on hydrogen. The exponents of the additional diffuse functions were generated in an even-tempered manner, starting with the most diffuse function in the original basis set. The exponents of the first additional basis functions: $\alpha(C,s) = 0.02201$, $\alpha(C,p) = 0.017845$, $\alpha(C,d) =$ $0.050000, \alpha(H,s) = 0.01263, \alpha(H,p) = 0.051000, \alpha(H,d)$ = 0.123500; the exponents of the subsequent sets were obtained according to $\alpha_{i+1} = 0.5 \cdot \alpha_i$.

We computed electronic resonances for C_2H^- with CAP-EOM-EE-CCSD/aug-cc-pVTZ+3s3p1d at the equilibrium geometry of the neutral, as well as stretched and bent geometries. Ground and excited states of C_2^- were computed using EOM-IP-CCSD/aug-cc-pVTZ with the dianionic [80] reference (C_2^{2-}), as described in detail in Ref. [80]. Core orbitals (1s_C) were frozen in all calculations. All calculations used pure angular momentum polarisation functions.

3. Results and discussion

3.1. Electronic structure of C₂

We begin by reviewing electronic states of C_2^- . To describe this open-shell molecule, we employ EOM-IP-CCSD with the dianion (C_2^{2-}) closed-shell reference. The dianionic reference is well-behaved (at least, up to the aug-cc-pVTZ basis) [80] and have been used to describe the electronic structure of C_2 , C_2^- , and C_2^{2-} .

Figure 2 shows molecular orbitals and electronic configuration of the ground electronic state of C_2^- ($X^2\Sigma_g^+$).



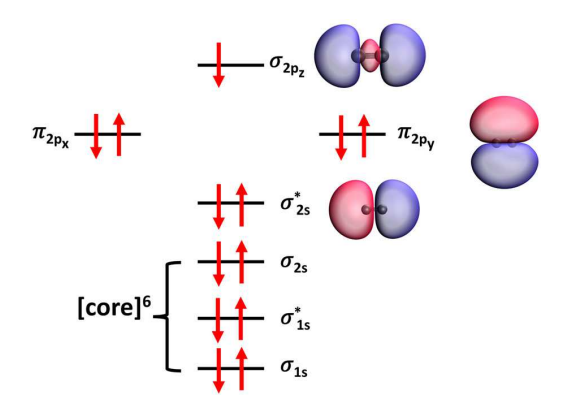
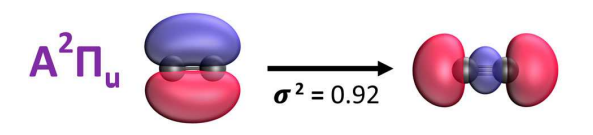


Figure 2. Molecular orbital diagram and electronic configuration of the ground electronic state of C_2^- . 'Core' denotes the three lowest molecular orbitals.



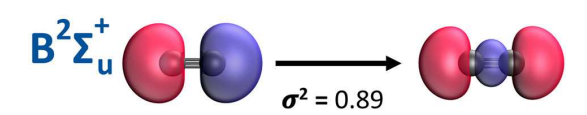


Figure 3. Natural transition orbitals for the $X^2\Sigma_a^+ \to A^2\Pi_u$ and $X^2\Sigma_q^+ \to B^2\Sigma_u^+$ transitions in C_2^- at the equilibrium geometry of C_2^- using EOM-IP-CCSD/aug-cc-pVTZ with the dianionic reference.

Table 1. Excitation energies and oscillator strengths for C_2^- at R_{CC} = 1.260 Å using EOM-IP-CCSD/aug-cc-pVTZ with the dianionic reference (C_2^{2-}) .

State	E _{ex} , eV	f
$A^2\Pi_{II}$	0.57	0.01
$A^2\Pi_u$ $B^2\Sigma_u^+$	2.45	0.09

Note that the singly occupied molecular orbital is of a σ -type and has a partial bonding character with respect to the two carbons. Table 1 shows the vertical excitation energy to $A^2\Pi_u$ and $B^2\Sigma_u^+$ obtained using EOM-IP-CCSD/aug-cc-pVTZ at the equilibrium geometry of C_2^- ($X^2\Sigma_g^+$). The computed energy gap between $X^2\Sigma_g^+$ and $B^2\Sigma_u^+$ is 2.45 eV, which is in perfect agreement with the fluorescence signal observed in the CVD experiment [40]. We also characterise the NTOs for excitation from the ground state of C_2^- ($X^2\Sigma_u^+$) to the $A^2\Pi_u$ and $B^2\Sigma_u^+$ excited states. NTOs are shown in Figure 3; their shapes are consistent with molecular orbitals and electronic configuration in Figure 2.

Recall that the motivation of this study comes from the experimental observation of fluorescence at 541 nm (2.28 eV) in a microwave-activated plasma; this transition corresponds to the emission from $B^2\Sigma_u^+$ to $X^2\Sigma_u^+$. Molecular orbital picture of this transition (shown in Figure 3) sets the parameters for the electronic structure of the precursor state. To form the excited state $(B^2\Sigma_u^+)$ of C_2^{-*} from an electronic resonance of C_2H^- , the precursor resonance state should have NTOs that are similar to the NTOs of $B^2\Sigma_u^+ \to X^2\Sigma_g^+$ transition shown in Figure 3: both should be of a σ -type, the hole NTO should have a node in the C-C bond and the particle NTO should have no node in the C-C bond. In a precursor state for the ground-state $C_2^-(X^2\Sigma_u^+)$ the NTOs should be of the same type, but the hole and particle NTOs should be reversed. In addition, the precursor states for forming C_2^- should have a node in the C-H bond, to yield a repulsive potential. These considerations guide our analysis of the C₂H⁻ resonances below.

3.2. Electronic structure of C₂H⁻

Molecular orbitals diagram and electronic configuration of the ground-state C₂H⁻ are shown in Figure 4. C₂H⁻ is a closed-shell anion, isoelectronic with CN⁻. The shapes of the orbitals are similar to those in C₂⁻ (Figure 2) and in CN⁻. Figure 5 shows computed detachment energies of the anion at different geometries. The ground state of C_2H corresponds to the detachment from a σ -type orbital, giving rise to the ${}^{2}\Sigma^{+}$ state, whereas the detachment from a π -type orbital gives rise to a higher $^2\Pi$ state; this pattern is similar to that of CN (see, for example, Ref. [35]), although the gap between the Σ and Π states is smaller in C₂H (0.7 eV versus 2 eV in CN). The computed VDE (3.02 eV) is close to the experimentally determined adiabatic detachment energy [81-83] (2.9-3.0 eV).

The continuum begins at the detachment threshold and electronic states above the threshold are the resonances. Resonances were computed with CAP-EOM-EE-CCSD at the equilibrium geometry of the neutral. Here we report resonance positions with respect to the ground state of the anion. Energies of the resonances with respect to the detachment threshold can be obtained by subtracting the VDE (3.02 eV). Table 2 lists all identified resonances below 10 eV; the corresponding η -trajectories are shown in the SI. The respective NTOs are shown in Table 3. C₂H⁻ is isoelectronic with CN⁻ and their lowlying states have similar character [35] - even the order of resonance states follows the same pattern. We identified 4 triplet resonances at 5.59-6.66 eV (2.57-3.64 eV above the threshold) and 2 singlet resonances at 6.7-6.8 eV (3.67–3.75 eV above the threshold). As in the CN⁻ case, the singlet resonances are broader than the triplet

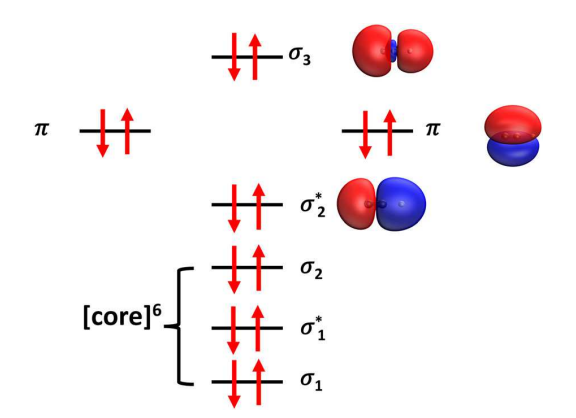


Figure 4. Molecular orbital diagram and electronic configuration of the ground electronic state of C_2H^- . 'Core' denotes the three lowest molecular orbitals. σ_2^* is of antibonding character with respect to CC and of bonding character with respect to CH.

ones. Qualitatively, our results agree with the *R*-matrix calculations of Harrison and Tennyson [84], although our symmetry assignments are different. The differences in resonance positions and widths between the 2 sets of calculations follow the same trends as in CN⁻ and cyanopolyyne anions and can be attributed to the different treatment of electron correlation [35].

Among these multiple resonances, there is none with a hole NTO that has a node in the C-C bond and particle NTO that has a node in the C-H bond. Hence, none of the computed resonances show dissociative (C-H) character and none correlate with either ground-state

Table 2. Resonance positions E_R (eV) and widths Γ (eV) at the equilibrium geometry of neutral C_2H using CAP-EOM-EE-CCSD/aug-cc-pVTZ+3s3p1d.

State	E _R ⁽⁰⁾	$\Gamma^{(0)}$	$E_R^{(1)}$	Γ ⁽¹⁾
$A^3\Sigma^+$	5.54	0.44	5.59	0.33
В ³ П	5.74	0.67	5.80	0.51
$C^3\Delta$	6.17	0.61	6.25	0.47
$D^3\Sigma^-$	6.61	0.86	6.66	0.77
$E^1\Sigma^-$	6.64	0.91	6.69	0.87
$F^1\Delta$	6.73	1.12	6.77	1.06

 $(X^2\Sigma_g^+)$ or excited $(B^2\Sigma_u^+)$ C_2^- . Because the character of the electronic state needs to change, one should anticipate a barrier along the dissociation coordinate.

In search of possible precursor states, we repeated the calculations at geometries with the stretched C-H bond. With C-H bond stretched by 0.6 Å (at $R_{CH} = 1.66$ Å), states of a desired orbital character (i.e. corresponding to excitations to σ and σ^* -type orbitals) appeared. The results of the calculation are summarised in Tables 4 and 5. The three lowest states show clear antibonding character with respect to the C-H bond. We observe two electronically bound states, $a^3\Sigma^+$ and $b^3\Pi$, derived by excitation from σ and π occupied orbitals to a σ^* -type orbital. These two states correlate electronically with the ground $(X^2\Sigma_g^+)$ or excited $(A^2\Pi_u)$ states of C_2^- . The $A^3\Sigma^+$ resonance starts to show a contribution of an additional NTO pair in which the hole orbital has a node in the C-C bond and the particle orbital has a node in the C-H bond and no node in the C-C bond. This means that this state can yield a repulsive C-H potential and electronically correlates with C_2^{-*} (B² Σ_u^+).

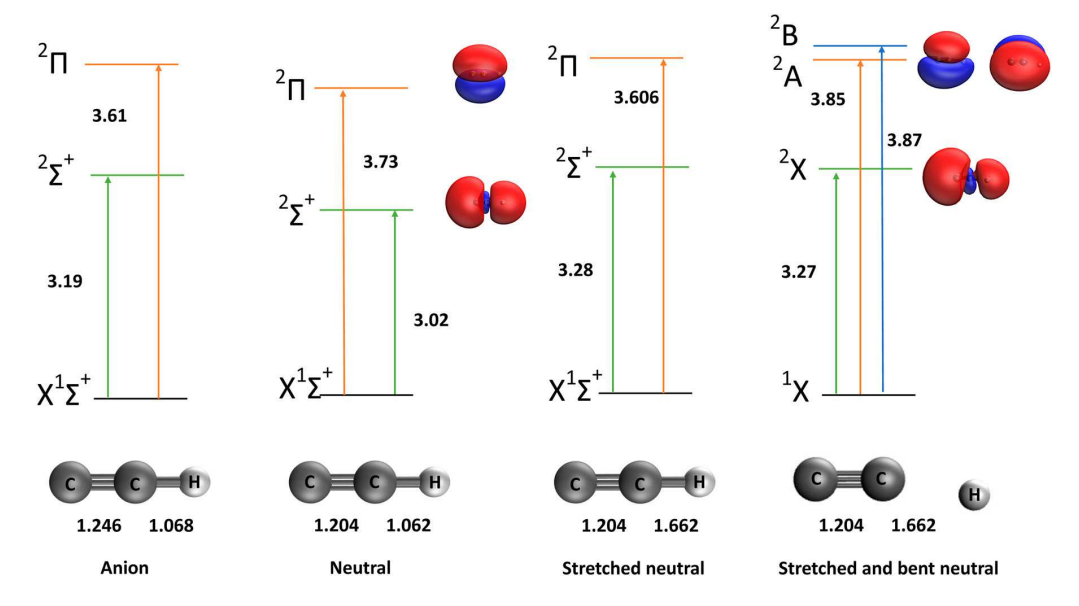


Figure 5. Vertical detachment energies and the respective Dyson orbitals of C₂H⁻ at different geometries.

Table 3. NTOs (real part)^a at the equilibrium geometry of the neutral ($R_{CC} = 1.204 \text{ Å}$ and $R_{CH} = 1.062 \text{ Å}$).

State	Туре	σ^2	Hole	Particle
$A^3\Sigma^+$	$\pi \to \pi^*$	0.454		***
		0.454		
B ³ Π	$\sigma o \pi^*$	0.894		
$C^3\Delta$ ($F^1\Delta$)	$\pi \to \pi^*$	0.451 (0.498)		
		0.451 (0.498)		8
$D^3\Sigma^-(E^1\Sigma^-)$	$\pi \to \pi^*$	0.468 (0.473)		
		0.468 (0.473)		

Note: a Singlet and triplet resonances have very similar NTOs, hence, only triplet NTOs are shown. The singular values are slightly different (singlet σ_{ν}^2 are shown in parenthesis).

Table 4. Resonance positions E_R (eV) and widths Γ (eV) at a stretched geometry ($R_{CC}\,=\,1.204$ Å and $R_{CH}\,=\,1.662$ Å); CAP-EOM-EE-CCSD/aug-cc-pVTZ+3s3p1d.

State	E _R ⁽⁰⁾	$\Gamma^{(0)}$	E _R ⁽¹⁾	Γ ⁽¹⁾
$a^3\Sigma^+$ (bound)	3.06	_	_	_
b ³ Π (bound)	3.14	-	-	_
$A^3\Sigma^+$	5.22	0.29	5.25	0.31
B ³ Π	5.92	0.73	5.81	0.57
$C^3\Delta$	6.22	0.68	6.13	0.55
$D^3\Sigma^-$	6.60	1.00	6.47	0.93
$E^1\Sigma^-$	6.61	1.09	6.48	1.00
$F^1\Delta$	6.65	1.24	6.49	1.16

To test the effect of bending vibration on the resonance position, we carried out calculations at a geometry with CCH bent at a stretched neutral geometry. The right panel in Figure 5 shows the vertical detachment energies and the corresponding Dyson orbitals at the bent and stretched neutral geometry. Table 6 shows the resonance positions and widths, and the respective NTOs are shown in Table 7. Due to symmetry lowering, the degeneracy of the Π states is lifted. Table 7 also compares each resonance with resonances obtained from just stretched geometry. Overall, bending does not seem to have significant effect on the character of the states and their energies.

To summarise, the resonance state $A^3\Sigma^+$ has all nodal features that can lead to a formation of excited C₂ $(B^2\Sigma_{ij}^+)$. We also observe that one of the bound excited states of C_2H^- ($a^1\Sigma^+$) correlates with the ground state

Table 5. NTOs (real part) at stretched geometry ($R_{CC} = 1.204$ Å and $R_{CH} = 1.662 \text{ Å.}$)

State	Type	σ^2	Hole	Particle
$a^3\Sigma^+$ (bound)	$\sigma ightarrow \sigma^*$	0.807	6 0	68
$b^3\Pi$ (bound)	$\pi o \sigma^*$	0.787		000
$A^3\Sigma^+$	$\sigma^* \to \sigma^*$	0.380		68
	$\pi o \pi^*$	0.261		98
	$\pi \to \pi^*$	0.261		

Table 6. Resonance positions E_R (eV) and widths Γ (eV) at a stretched and bent geometry (R $_{CC}=1.204\,\text{Å}$, R $_{CH}=1.662\,\text{Å}$, and \angle CCH = 170°); CAP-EOM-EE-CCSD/aug-cc-pVTZ+3s3p1d.

State	$E_R^{(0)}$	$\Gamma^{(0)}$	$E_R^{(1)}$	Γ ⁽¹⁾
a ³ A' (bound)	3.00	_	_	_
b^3A' (bound)	3.14	-	-	_
c^3A'' (bound)	3.12	-	-	_
A^3A'	5.25	0.29	5.23	0.27
B^3A'	5.85	0.70	5.79	0.60
C^3A''	5.92	0.73	5.81	0.57
D^3A''	6.25	0.74	6.17	0.59
E^3A''	6.60	1.09	6.49	1.03

of C_2^- ($X^2\Sigma_g^+$), while another correlates with the $A^2\Pi_u$

Figure 6 shows an overview of the low-lying electronic states at the three different geometries. On the left panel, the electronic states of the C₂H⁻ anion at the neutral geometry are shown. The middle panel shows the electronic states of C₂H⁻ anion with a stretched C-H bond. The ground state of the stretched C₂H⁻ is higher than the ground state of C₂H⁻, which shifts all states to higher energy. At this geometry, the character of the states changes and the 3 lowest states show an antibonding C-H character. The two lowest states are electronically bound (vertically) and correlate with the two lowest states of C_2^- . The third state, $A^3\Sigma^+$, is a resonance with electronic configuration that correlates with the $B^2\Sigma_u^+$ state of C_2^{-*} . The right panel of Figure 6 shows the ground and excited states of C₂⁻ relative to the ground state of C₂H⁻ anion (to compare energy of C₂⁻ with C₂H⁻, the energy of hydrogen atom, -0.5 hartree, was added to the energy of C_2^-). The comparison of these states allows us to establish a correlation diagram suggesting the formation of the ground-state of C_2^- via the $a^3\Sigma^+$ bound excited state of C_2H^- and formation of the excited state of C_2^{-*} ($^2\Sigma_{\mu}^+$) via the $A^3\Sigma^+$ resonance state of C_2H^- .

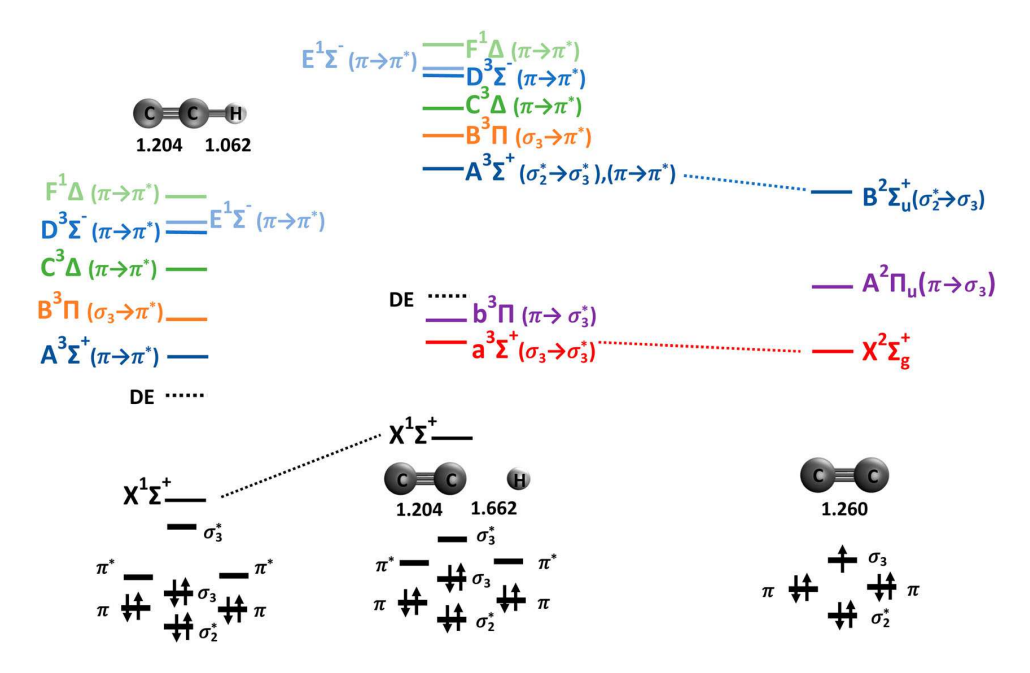


Figure 6. Right: Electronic states of C_2H^- at the ground state equilibrium geometry of the of the neutral. Middle: Electronic states of C_2H^- at the geometry with an elongated C-H bond. Left: Electronic states of C_2^- at the equilibrium geometry of C_2^- ($X^2\Sigma_a^+$).

To estimate relative energies more accurately, we computed energy differences between the total energies of the lowest state of the anions at the 3 geometries: groundstate neutral C₂H (as in panel 2 in Figure 6), the geometry with a stretched C-H bond (as in panel 3 in Figure 6), and at the dissociation limit (as in panel 4 in Figure 6); the respective energies are given in Table S7 in the SI. This calculation shows that the ground electronic state of the anion with the stretched bond is 2.519 eV above the ground electronic state of the anion at the equilibrium geometry of the neutral ground state. The dissociation limit (C_2^- ($X^2\Sigma_g^+$) + H) is 5.289 eV above and the excited-state dissociation limit (C_2^- ($B^2\Sigma_u^+$) + H) is 7.744 eV above the ground-state energy of C₂H⁻ at the equilibrium geometry of the neutral. Hence, all resonances below 10 eV (see Table 2) have enough energy to produce ground-state C_2^- , but not C_2^- ($B^2\Sigma_u^+$). For this channel to open up, additional $\sim\!2$ eV are needed. We note that the experiment was carried out in high-energy plasma, which was microwave activated. Thus, electron attachment to rotationally and vibrationally hot molecules could lead to the formation of C_2^- ($B^2\Sigma_u^+$). If the bond is already stretched up to 1.662 Å (which is equivalent to imparting 2.8 eV to the neutral C_2H or 2.5 eV to the C_2H^-) then resonances above 5.2 eV (vertically) can lead to the formation of excited C₂⁻. Although the temperature of the plasma in the CVD experiment [40] is an order of magnitude lower than the required amount (2,900 K versus 29,000 K \approx 2.5 eV), there should be sufficient number of highly energetic molecules capable of forming C_2^{-*} . Indeed, by using the Maxwell-Boltzmann distribution, we estimate that 0.02% of molecules have energy above 29,000 K.

We note that the shape of the potential energy surfaces of C_2H and C_2H^- (as well as larger species from this family) has implications for astrochemical routes of formation of carbon-chain anions [85].

This observed pattern is suggestive of multiple processes initiated by the electron capture by C₂H. Attachment of electrons with energies below 10 eV to cold molecules can lead to multiple resonances of π^* type, which can inter-convert in the course of non-adiabatic dynamics. For example, a π -type resonance can undergo a transition to a σ -type resonance. Energetically, all identified resonances can lead to the C-H bond fission and the formation of the ground-state C2. However, the excitedstate channel require additional 2.5 eV of energy; hence, it can be accessed only by electron attachment to highly energetic molecules. Importantly, none of the resonances identified at the equilibrium geometry of C2H correlate electronically to either C_2^- or C_2^{*-} ; only when C-H bond is sufficiently stretched, the resonance states of the desired orbital character appear. This suggests that the formation of C_2^-/C_2^{*-} can occur either diabatically, via electron capture by the molecules with stretched C-



Table 7. NTOs (real part) at stretched and bent geometry (R_{CC} = 1.204 Å, $R_{CH} = 1.662$ Å, and $\angle CCH = 170^{\circ}$).

0 ,			., 0 ,.	
State	$SVD(\sigma^2)$	Hole	Particle	Correlates with
³ A' (bound)	0.790			$^3\Sigma^+$
³ A' (bound)	0.785			³П
³ <i>A</i> " (bound)	0.789			³П
³ A'	0.421			$^3\Sigma^+$
	0.209			
	0.240			
³ A'	0.714		%	³П
	0.162			
³ A"	0.876			³П
³ A"	0.464			$^3\Delta$
	0.444			
³ A"	0.461			³ ∑ [−]
	0.493			

Note: ^a Correlation between states at the bent and stretched geometry with states obtained at the linear geometry.

H bonds into $a^3\Sigma^+$ or $A^3\Sigma^+$, or non-adiabatically, by forming another type of a resonance that, given sufficient energy, can adiabatically evolve into the desired state.

This is reminiscent of the proposed mechanism of double-strand breaking in DNA [4-7]: it is believed that the capture of the electron proceeds via a π^* -type resonance that undergoes a non-adiabatic transition to a σ^* type resonance leading to eventual bond-breaking. This motif is also similar to photochemical bond breaking in aromatic molecules, such as pyrrole: the essential feature of photoinduced dynamics [86] in many heteronuclear aromatic compounds is that the initial excitation to the bright ${}^{1}\pi\pi^{*}$ state eventually leads to the X-H bond breaking via non-adiabatic transition to a $\sigma\sigma^*$ state.

4. Conclusion

We presented a detailed electronic structure analysis of the bound and metastable states in C₂H⁻. The calculations were carried out using high-level electronic structure methods adapted to describe both bound and metastable states on the same footing. By analysing the characters of the states by means of NTOs, we identified possible precursor states that can lead to the formation of the ground-state and electronically excited C₂ observed in carbon-rich plasmas. To fully elucidate the mechanism of DEA requires dynamics simulations, including non-adiabatic transitions, and we hope that our results lay a ground-work for future, more detailed investigations of DEA. By studying DEA in C₂H⁻, we identified intriguing similarities with DEA and photochemical processes in more complex systems (aromatic heterocycles). This study contributes towards better understanding of electron-induced processes occurring in nature and explored in existing and emerging technologies.

Disclosure statement

A.I.K. is the president and a part-owner of Q-Chem, Inc. No potential conflict of interest was reported by S. G.

Funding

This work was supported by NSF [CHE-1856342].

ORCID

Sahil Gulania http://orcid.org/0000-0001-7918-6669 Anna I. Krylov Dhttp://orcid.org/0000-0001-6788-5016

References

- [1] C.R. Arumainayagam, H.-L. Lee, R.B. Nelson, D.R. Haines and R.P. Gunawardane, Surf. Sci. Rep. 65, 1 (2010). doi:10.1016/j.surfrep.2009.09.001
- [2] H. Chevreau, F. Gardebien, C. Dezarnaud-Dandine and A. Sevin, Chem. Phys. Chem. 2, 583 (2001). doi:10.1002/(ISSN)1439-7641
- J. Michl and V. Bonačić-Koutecký, Electronic Aspects of Organic Photochemistry (Wiley, New York, 1990).
- [4] J. Simons, J. Phys. Chem. A. 112, 6401 (2008). doi:10.1021/
- [5] J. Simons, Annu. Rev. Phys. Chem. 62, 107 (2011). doi:10.1146/annurev-physchem-032210-103547
- J. Simons, in Photoionization and Photodetachment, edited by C.Y, Ng, Vol. 10, Part II; Advanced Series in Physical Chemistry. World Scientific Publishing Co., Singapore, 2000.
- [7] J.M. Herbert, Rev. Comp. Chem. 28, 391 (2015). doi: 10.1002/9781118889886.ch8.
- [8] B. Boudaïffa, P. Cloutier, D. Hunting, M.A. Huels and L. Sanche, Science 287, 1658 (2000). doi:10.1126/science. 287.5458.1658

- [9] J. Simons, Acc. Chem. Res. 39, 772 (2006). doi:10.1021/ar
- [10] B.M. Penetrante, M.C. Hsiao, J.N Bardsley, B.T. Merritt, G.E. Vogtlin, A. Kuthi, C.P. Burkhart and J.R. Bayless, Plasma Sources Sci. Technol. 6, 251 (1997). doi:10.1088/0963-0252/6/3/002
- [11] T. Matsumoto, D.Y. Wang, T. Namihira and H. Akiyama, IEEE Trans. Plasma Sci. 38, 2639 (2010). doi:10.1109/ TPS.2010.2045903
- [12] P. Rumbach and D.B. Go, Topics in Catalysis, Vol. 56, chapter Perspectives on Plasmas in Contact with Liquids for Chemical Processing and Materials Synthesis. (Springer, 2013).
- [13] S.M. Thagard, G.R. Stratton, F. Dai, C.L. Bellona, T.M. Holsen, D.G. Bohl, E. Paek and E.R.V. Dickenson, J. Phys. D: Appl. Phys. 50, 014003 (2017). doi:10.1088/1361-6463/50/1/014003
- [14] P. Mehta, P. Barboun, F.A. Herrera, J. Kim, P. Rumbach, D.B. Go, J.C. Hicks and W.F. Schneider, Nature Cat. 1, 269 (2018). doi:10.1038/s41929-018-0045-1
- [15] G. Yoon, I. Kim, S. So, J. Mun, M. Kim and J. Rho, Sci. Rep. 7, 6668 (2017). doi:10.1038/s41598-017-06833-5
- [16] G.A. Olah, Acc. Chem. Res. 20, 422 (1987). doi:10.1021/ ar00143a006
- J.H. Lunsford, Angew. Chem., Int. Ed. 34, 970 (1995). doi:10.1002/(ISSN)1521-3773
- [18] J. Kim, D.B. Go and J.C. Hicks, Phys. Chem. Chem. Phys. 19, 13010 (2017). doi:10.1039/C7CP01322A
- [19] P. Rumbach, R. Xu and D.B. Go, J. Electrochem. Soc. 163, F1157 (2016). doi:10.1149/2.0521610jes
- [20] A. Studer and D.P. Curran, Nat. Chem. 6, 765 (2014). doi:10.1038/nchem.2031
- [21] A. Houmam, Chem. Rev. 108, 2180 (2008). doi:10.1021/
- [22] W.P. Reinhardt, Annu. Rev. Phys. Chem. 33, 223 (1982). doi:10.1146/annurev.pc.33.100182.001255
- [23] N. Moiseyev, Phys. Rep. 302, 212 (1998). doi:10.1016/S03 70-1573(98)00002-7
- [24] N. Moiseyev, Non-Hermitian Quantum Mechanics (Cambridge University Press, Israel Institute of Technology, Haifa, 2011).
- [25] T.-C. Jagau, K.B. Bravaya and A.I. Krylov, Annu. Rev. Phys. Chem. 68, 525 (2017). doi:10.1146/annurev-physch em-052516-050622
- [26] A.I. Krylov, Annu. Rev. Phys. Chem. 59, 433 (2008). doi:10.1146/annurev.physchem.59.032607.093602
- [27] K. Sneskov and O. Christiansen, WIREs: Comput. Mol. Sci. 2, 566 (2012). doi:10.1002/wcms.99
- [28] R.J. Bartlett, WIREs: Comput. Mol. Sci. 2, 126 (2012). doi:10.1002/wcms.76
- [29] A. Dreuw and M. Wormit, WIREs: Comput. Mol. Sci. 5, 82 (2015). doi:10.1002/wcms.1206
- [30] S. Klaiman and I. Gilary, Adv. Quantum Chem. 63, 1 (2012). doi:10.1016/B978-0-12-397009-1.00001-1
- [31] M. Ehara and T. Sommerfeld, Chem. Phys. Lett. 537, 107 (2012). doi:10.1016/j.cplett.2012.03.104
- [32] T.-C. Jagau, D.B. Dao, N.S. Holtgrewe, A.I. Krylov and R. Mabbs, J. Phys. Chem. Lett. 6, 2786 (2015). doi:10.1021/acs.jpclett.5b01174
- [33] J. Lyle, T.-C. Jagau and R. Mabbs, Faraday Discuss. 217, 533 (2019). doi:10.1039/C8FD00224J

- [34] S. Gulania, T.-C. Jagau, A. Sanov and A.I. Krylov, Phys. Chem. Chem. Phys. 22, 5002-5010 (2020). doi:10.1039/ C9CP06484B
- [35] W. Skomorowski, S. Gulania and A.I. Krylov, Phys. Chem. Chem. Phys. 20, 4805 (2018). doi:10.1039/C7CP08227D
- [36] Z. Benda and T.-C. Jagau, J. Chem. Theory Comput. 14, 4216 (2018). doi:10.1021/acs.jctc.8b00444
- [37] A.A. Kunitsa and K.B. Bravaya, J. Phys. Chem. Lett. 6, 1053 (2015). doi:10.1021/acs.jpclett.5b00207
- [38] G. Jolicard and E.J. Austin, Chem. Phys. Lett. 121, 106 (1985). doi:10.1016/0009-2614(85)87164-5
- [39] U.V. Riss and H.-D. Meyer, J. Phys. B 26, 4503 (1993). doi:10.1088/0953-4075/26/23/021
- [40] E.J.D. Mahoney, B.S. Truscott, M.N.R. Ashfold and Yu. A. Mankelevich, J. Phys. Chem. A 121, 2760 (2017). doi:10.1021/acs.jpca.7b00814
- [41] M.C. McCarthy, C.A. Gottlieb, H. Gupta and P. Thaddeus, J. Lett. 652, L141 (2006). doi:10.1086/510238
- [42] S. Brünken, H. Gupta, C.A. Gottlieb, M.C. McCarthy and P. Thaddeus, J. Lett. 664, L43 (2007). doi:10.1086/520703
- [43] P. Thaddeus, C.A. Gottlieb, H. Gupta, S. Brünken, M.C. McCarthy, M. Agúndez, M. Guelin and J. Cernicharo, Astrophys. J. 677, 1132 (2008). doi:10.1086/529125
- [44] J. Cernicharo, M. Guélin, M. Agundez, K. Kawaguchi, M. McCarthy and P. Thaddeus, Astron. Astrophys. 467, L37 (2007). doi:10.1051/0004-6361:20077415
- [45] J. Cernicharo, M. Guélin, M. Agundez, M.C. McCarthy and P. Thaddeus, Astrophys. J. Lett. 688, L83 (2008). doi:10.1086/595583
- [46] M. Agúndez, J. Cernicharo, M. Guélin, C. Kahane, E. Roueff, J. Kłos, F.J. Aoiz, F. Lique, N. Marcelino, J.R. Goicoechea, M. González-Garcia, C.A. Gottlieb, M.C. McCarthy and P. Thaddeus, Astron. Astrophys. 517, L2 (2010). doi:10.1051/0004-6361/201015186
- [47] B.A. McGuire, A.M. Burkhardt, S. Kalenskii, C.N. Shingledecker, A.J. Remijan, E. Herbst and M.C. McCarthy, Science 359, 202 (2018). doi:10.1126/science.aao4890
- [48] W.H.A Wollaston, Philos. Trans. R. Soc. London 92, 365 (1802). doi:10.1098/rstl.1802.0014
- [49] A.N. Goyette, J.E. Lawler, L.W. Anderson, D.M. Gruen, T.G. McCauley, D. Zhou and A.R. Krauss, J. Phys. D: Appl. Phys. 31, 1975 (1998). doi:10.1088/0022-3727/31/16/
- [50] N.J. Reilly, T.W. Schmidt and S.H. Kable, J. Phys. Chem. A. 110, 12355 (2006). doi:10.1021/jp064411z
- [51] E. Szymańska, I. Čadež, E. Krishnakumar, and N.J. Mason, Phys. Chem. Chem. Phys. 16, 3425 (2014). doi:10.1039/C3CP54459A
- K. Emrich, Nucl. Phys. A351, 379 (1981). doi:10.1016/ 0375-9474(81)90179-2
- [53] H. Sekino and R.J. Bartlett, Int. J. Quant. Chem. 26, 255 (1984). doi:10.1002/(ISSN)1097-461X
- [54] H. Koch and P. Jørgensen, J. Chem. Phys. 93, 3333 (1990). doi:10.1063/1.458814
- [55] H. Koch, H.J. Aa, H.J.Aa Jensen, P. Jørgensen and T. Helgaker, J. Chem. Phys. 93, 3345 (1990). doi:10.1063/1. 458815
- [56] J.F. Stanton and R.J. Bartlett, J. Chem. Phys. 98, 7029 (1993). doi:10.1063/1.464746
- [57] M. Nooijen and R.J. Bartlett, J. Chem. Phys. 102, 6735 (1995). doi:10.1063/1.469147



- [58] S.V. Levchenko and A.I. Krylov, J. Chem. Phys. 120, 175 (2004). doi:10.1063/1.1630018
- [59] A.I. Krylov, in Reviews in Comp. Chem., edited by A. L. Parrill and K. B. Lipkowitz (J. Wiley & Sons, 2017), Vol. 30, pp. 151-224.
- [60] T. Helgaker, P. Jørgensen and J. Olsen, Molecular Electronic Structure Theory (Wiley & Sons, 2000).
- [61] D. Zuev, T.-C. Jagau, K.B. Bravaya, E. Epifanovsky, Y. Shao, E. Sundstrom, M. Head-Gordon and A.I. Krylov, J. Chem. Phys. 141, 024102 (2014). doi:10.1063/1.4885056
- [62] T.-C. Jagau, D. Zuev, K.B. Bravaya, E. Epifanovsky and A.I. Krylov, J. Phys. Chem. Lett. 5, 310 (2014). doi:10.1021/jz402482a
- [63] T.-C. Jagau and A.I. Krylov, J. Phys. Chem. Lett. 5, 3078 (2014). doi:10.1021/jz501515j
- [64] T.-C. Jagau and A.I. Krylov, J. Chem. Phys. 144, 054113 (2016). doi:10.1063/1.4940797
- [65] W. Skomorowski and A.I. Krylov, J. Phys. Chem. Lett. 9, 4101 (2018). doi:10.1021/acs.jpclett.8b01794
- [66] R. Santra and L.S. Cederbaum, Phys. Rep. 368, 1 (2002). doi:10.1016/S0370-1573(02)00143-6
- [67] A.I. Krylov, J. Chem. Phys. 153, 080901 (2020). doi:10. 1063/5.0018597
- [68] J.V. Ortiz, J. Chem. Phys. 153, 070902 (2020). doi:10.1063/ 5.0016472
- [69] A.V. Luzanov, A.A. Sukhorukov and V.E. Umanskii, Theor. Exp. Chem. 10, 354 (1976). doi:10.1007/BF00526 670Russian original: Teor. Eksp. Khim., 10, 456 (1974).
- [70] A.V. Luzanov and V.F. Pedash, Theor. Exp. Chem. 15, 338 (1979). doi:10.1007/BF00520694
- [71] A.V. Luzanov and O.A. Zhikol, in Practical aspects of computational chemistry I: An overview of the last two decades and current trends, edited by J. Leszczynski and M.K. Shukla (Springer, 2012), pp. 415-449.
- [72] F. Plasser, M. Wormit and A. Dreuw, J. Chem. Phys. 141, 024106 (2014). doi:10.1063/1.4885819
- [73] F. Plasser, S.A. Bäppler, M. Wormit and A. Dreuw, J. Chem. Phys. 141, 024107 (2014). doi:10.1063/1.488
- [74] S. Mewes, F. Plasser, A. Krylov and A. Dreuw, J. Chem. Theory Comput. 14, 710 (2018). doi:10.1021/acs.jctc.
- [75] S. Matsika, X. Feng, A.V. Luzanov and A.I. Krylov, J. Phys. Chem. A 118, 11943 (2014). doi:10.1021/jp506090g
- [76] A.I. Krylov and P.M.W. Gill, WIREs: Comput. Mol. Sci. 3, 317 (2013). doi:10.1002/wcms.1122
- [77] Y. Shao, Z. Gan, E. Epifanovsky, A.T.B. Gilbert, M. Wormit, J. Kussmann, A.W. Lange, A. Behn, J. Deng, X. Feng, D. Ghosh, M. Goldey, P.R. Horn, L.D. Jacobson, I. Kaliman, R.Z. Khaliullin, T. Kus, A. Landau, J. Liu, E.I. Proynov, Y.M. Rhee, R.M. Richard,

- M.A. Rohrdanz, R.P. Steele, E.J. Sundstrom, H.L. Woodcock III, P.M. Zimmerman, D. Zuev, B. Albrecht, E. Alguires, B. Austin, G.J.O. Beran, Y.A. Bernard, E. Berquist, K. Brandhorst, K.B. Bravaya, S.T. Brown, D. Casanova, C.-M. Chang, Y. Chen, S.H. Chien, K.D. Closser, D.L. Crittenden, M. Diedenhofen, R.A. DiStasio Jr., H. Do, A.D. Dutoi, R.G. Edgar, S. Fatehi, L. Fusti-Molnar, A. Ghysels, A. Golubeva-Zadorozhnaya, J. Gomes, M.W.D. Hanson-Heine, P.H.P. Harbach, A.W. Hauser, E.G. Hohenstein, Z.C. Holden, T.-C. Jagau, H. Ji, B. Kaduk, K. Khistyaev, J. Kim, J. Kim, R.A. King, P. Klunzinger, D. Kosenkov, T. Kowalczyk, C.M. Krauter, K.U. Laog, A. Laurent, K.V. Lawler, S.V. Levchenko, C.Y. Lin, F. Liu, E. Livshits, R.C. Lochan, A. Luenser, P. Manohar, S.F. Manzer, S.-P. Mao, N. Mardirossian, A.V. Marenich, S.A. Maurer, N.J. Mayhall, C.M. Oana, R. Olivares-Amaya, D.P. O'Neill, J.A. Parkhill, T.M. Perrine, R. Peverati, P.A. Pieniazek, A. Prociuk, D.R. Rehn, E. Rosta, N.J. Russ, N. Sergueev, S.M. Sharada, S. Sharmaa, D.W. Small, A. Sodt, T. Stein, D. Stuck, Y.-C. Su, A.J.W. Thom, T. Tsuchimochi, L. Vogt, O. Vydrov, T. Wang, M.A. Watson, J. Wenzel, A. White, C.F. Williams, V. Vanovschi, S. Yeganeh, S.R. Yost, Z.-Q. You, I.Y. Zhang, X. Zhang, Y. Zhou, B.R. Brooks, G.K.L. Chan, D.M. Chipman, C.J. Cramer, W.A. Goddard III, M.S. Gordon, W.J. Hehre, A. Klamt, H.F. Schaefer III, M.W. Schmidt, C.D. Sherrill, D.G. Truhlar, A. Warshel, X. Xu, A. Aspuru-Guzik, R. Baer, A.T. Bell, N.A. Besley, J.-D. Chai, A. Dreuw, B.D. Dunietz, T.R. Furlani, S.R. Gwaltney, C.-P. Hsu, Y. Jung, J. Kong, D.S. Lambrecht, W.Z. Liang, C. Ochsenfeld, V.A. Rassolov, L.V. Slipchenko, J.E. Subotnik, T. Van Voorhis, J.M. Herbert, A.I. Krylov, P.M.W. Gill and M. Head-Gordon, Mol. Phys. 113, 184 (2015). doi:10.1080/00268976.2014.952696
- [78] T.H. Dunning Jr., J. Chem. Phys. 90, 1007 (1989). doi:10.1063/1.456153
- R.A. Kendall, T.H. Dunning and R. J. Harrison Jr., J. Chem. Phys. 96, 6796 (1992). doi:10.1063/1.462569
- S. Gulania, T.-C. Jagau and A.I. Krylov, Faraday Discuss. 217, 514 (2019). doi:10.1039/C8FD00185E
- [81] B.K. Janousek, J.I. Brauman and J. Simons, J. Chem. Phys. 71, 2057 (1979). doi:10.1063/1.438597
- [82] K.M. Ervin and W.C. Lineberger, J. Phys. Chem. 95, 1167 (1991). doi:10.1021/j100156a026
- [83] T.R. Taylor and C.S. Xu, J. Chem. Phys. 108, 10018 (1998). doi:10.1063/1.476462
- [84] S. Harrison and J. Tennyson, J. Phys. B 44, 045206 (2011). doi:10.1088/0953-4075/44/4/045206
- M.L. Senent and M. Hochlaf, Astrophys. J. 768, 59 (2013). doi:10.1088/0004-637X/768/1/59
- M.N.R. Ashfold, G.A. King, D. Murdock, M.G.D. Nix, T.A.A. Oliver and A.G. Sage, Phys. Chem. Chem. Phys. 12, 1218 (2010). doi:10.1039/B921706A